Journal of Solid State Chemistry **154,** 626–634 (2000)
doi:10.1006/jssc.2000.8906, available online at http://www.idealibrary.com on IDEAL®

$K_{7.62(1)}Si_{46}$ and $Rb_{6.15(2)}Si_{46}$: Two Structure I Clathrates with Fully Occupied Framework Sites

Ganesh K. Ramachandran[1,*] and Paul F. McMillan[1,*]

Department of Chemistry & Biochemistry, and Center for Solid State Science, Arizona State University, Tempe, Arizona 85287

and

Jianjun Dong and Otto F. Sankey

Department of Physics & Astronomy, and Materials Research Center, Arizona State University, Tempe, Arizona 85287

Received June 1, 2000; in revised form July 12, 2000; accepted July 28, 2000; published online September 30, 2000

We report here the synthesis and structural characterization of two Structure I clathrates in the K–Si and Rb–Si systems. As observed previously for Na_8Si_{46}, the alkali-Si clathrates are fully stoichiometric at the framework sites, i.e., devoid of framework vacancies. This is in sharp contrast to the analogous K–Ge, Rb–Ge, and Rb–Sn, (K,Cs)–Sn, and Cs–Sn systems, where two vacancies are formed predominantly at one-third of the crystallographic 6*c* tetrahedral sites (the formation of vacancies is rationalized to remove the tetrahedral atom of its hypervalency). This result is understood generally in terms of weaker *Tt*–*Tt* (*Tt* (tetrelide) = Si, Ge, Sn) bonding as one descends the periodic table. Also observed are metallic conductivities for both K_8Si_{46} and Rb_6Si_{46}, substantiating further the absence of vacancies — the "extra" electrons from the guest atoms participate in the conduction bands of the Si network, resulting in conductivities typical of semimetals. This is contrasted with the semiconducting behavior of the vacancy bearing K_8Ge_{44} ($K_8Ge_{44}\square_2$). © 2000 Academic Press

INTRODUCTION

Group IV analogs of the Structure I and II clathrate hydrates have received increasing attention over the past several years, following the observation of unusual and interesting properties of these materials, including superconductivity in these endohedrally substituted fuller*ane*-like structures (1), prediction (2–5) followed by measurement (6) of a wide ($\sim$2 eV) optical band gap in this family of Si-based "expanded volume" frameworks, and prediction (7) and attainment of promising values of the electrical and thermal conductivities for thermopower applications (8–16). More recently, the similarity of high-pressure behavior of Si_{136}-based frameworks (17–18) with that of elemental Si, as well as the high-pressure synthesis of these low-density frameworks (19), has sparked additional interest. The frameworks built from Group IV (Si, Ge, Sn) elements adopt cage-like structures around guest atoms, usually from Groups I or II (alkali or alkaline-earth metal atoms), that are incorporated during the synthesis and that possibly act as "templates" for the formation of the open framework structures. The cages in the Group IV clathrate structures observed to date define dodecahedral, tetrakaidecahedral, and hexakaidecahedral sites for the guest metal atoms (given symbols X, R, and Q, respectively). At present, only two clathrate types, with general formulae $X_2R_6Tt_{46}$ and $X_{16}Q_8Tt_{136}$ (Tt is an atom of Group IV, or tetrel; X, R, and Q are the polyhedral sites described above), have been described experimentally (20–25). Although several other clathrate structures, with comparable energetics, have been predicted to exist on theoretical grounds (26), these have not been experimentally realized yet. Interesting combinations of both types of clathrate, with various Group III–Group IV framework stoichiometries, in combination with various choices of alkali/alkaline-earth guest atoms, have now been prepared (27–34). We focus here on characterizing the relationship between the structural chemistry and the electronic conductivity in Structure I clathrates of silicon, containing alkali metal atoms as guests and the Structure I clathrate of germanium, containing potassium, as guest.

The Structure I clathrates of Si, Ge, and Sn are characterized by the presence of fused fullerane-like polyhedra, namely dodecahedra ($Tt_{20} \equiv X$) and tetrakaidecahedra ($Tt_{24} \equiv R$). There are two smaller Tt_{20} and six larger Tt_{24} units in each unit cell of the simple cubic structure (space group

[1] Please address correspondence to Ganesh K. Ramachandran (krg@asu.edu) and Paul F. McMillan (pmcmillan@asu.edu).

*Present address: Department of Chemistry, University College London, and The Royal Institution of Great Britain, 21 Albemarle Street, London W1X 4BS, UK.

0022-4596/00 $35.00

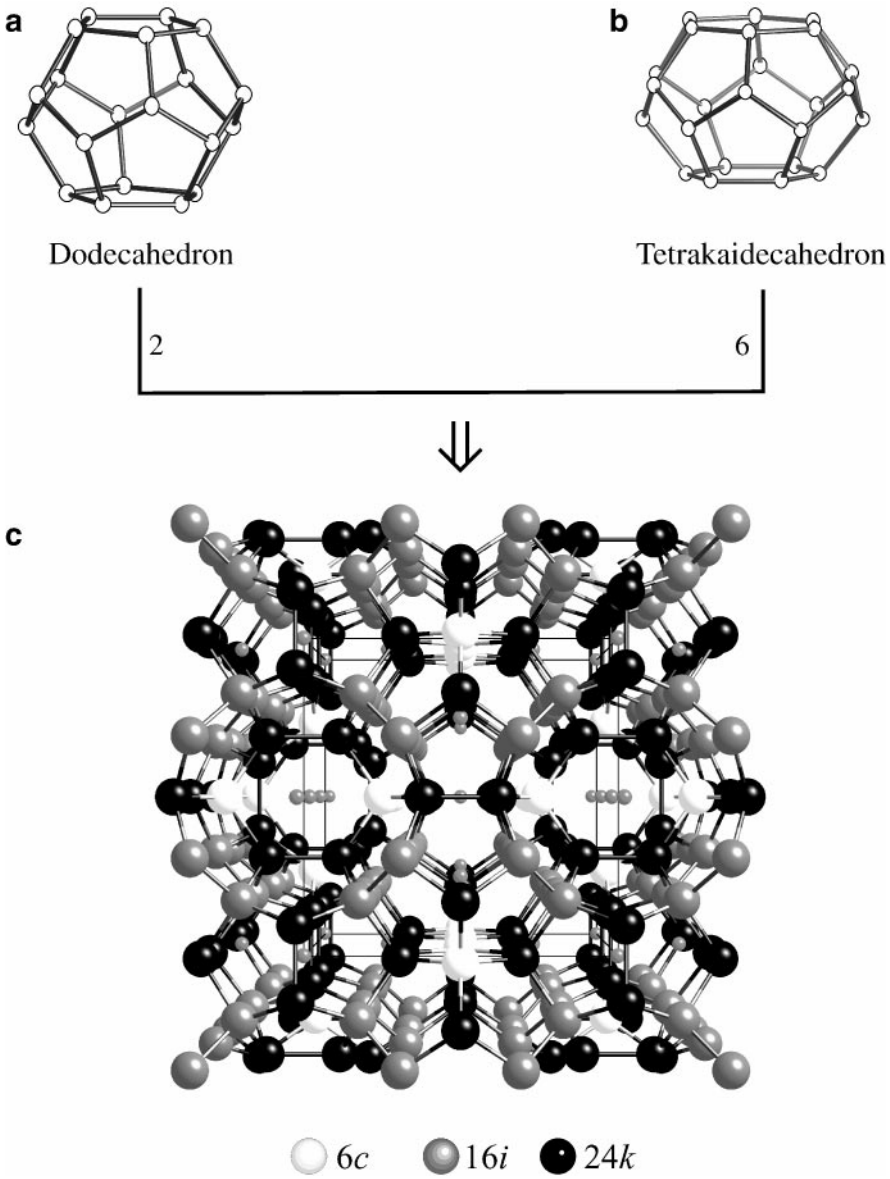

FIG. 1. Building blocks of the Structure I clathrate. (a) A dodecahedron consists of 12 faces and 20 vertices (Tt_{20}), and (b) a tetrakaidecahedron consists of 14 faces and 24 vertices (Tt_{24}). The overall structure, shown along the [100] direction is built by fusing Tt_{20} and Tt_{24} in the ratio 2:6 through five- and six-membered windows. There are three inequivalent crystallographic sites for the framework atoms, 6*c*, 16*i*, and 24*k*, in the Wyckoff notation and are shown in varying shades of gray. The void at the centers of the polyhedra provide residence for guest alkali (alkaline-earth) metal atoms.

$Pm\bar{3}n$, No. 223). In the ideal structures (i.e., without framework vacancies), all Tt atoms are tetrahedrally bound to each other, forming an open framework solid containing a large number (86%) of five-membered rings (Fig. 1). There are three crystallographically inequivalent sites for the four-coordinated framework atoms, namely 6*c*, 16*i*, and 24*k*, in the Wyckoff notation. The two nonframework sites, 2*a* and 6*d*, are the centers of the Tt_{20} and Tt_{24} polyhedra, respectively, and define the positions of the guest metal atoms.

The stoichiometry of the Structure I clathrate in the A_8Tt_{46} structure (A = Na, K, Rb, Cs) has been the subject of discussion (35–37) for some time. Much of this discussion has centered around the conflict between the reported compositions which generally correspond to ideal stoichiometries (21, 24–25), and their observed electrical behavior. According to classical electron counting rules, fully stoichiometric A_8Tt_{46} frameworks should be electron-rich, because of the additional electrons donated by the electropositive metal atoms. The total valence electron count suggests that the Tt atoms are hypervalent (i.e., 192/46 = 4.17 electrons per Tt atom). Following the Zintl-Klemm concept, the formation of two vacancies in the framework

structure, i.e., $A_8Tt_{44}\square_2$, would allow the accommodation of the eight extra electrons from the alkali metals (A) onto the framework, while maintaining electroneutrality (35, 36). Zhao and Corbett (37) demonstrated the existence of this phenomenon for Structure I clathrates (actually, "ionic" Zintl phases) in the Rb–Sn and the pseudobinary (K,Cs)–Sn systems. From careful X-ray studies, they concluded that the stoichiometries were $Rb_8Sn_{44}\square_2$ and $(K,Cs)_8Sn_{44}\square_2$, respectively, *and not* Rb_8Sn_{46} and $(K,Cs)_8Sn_{46}$ as the ideal stoichiometry would suggest. Cohn *et al.* (9) likewise reported the composition of the corresponding Cs–Sn clathrate to be $Cs_8Sn_{44}\square_2$. The Zintl-Klemm model offers a simple explanation for the formation of many Structure I clathrate compounds with partial substitutions on the framework and guest atom sites, i.e., $A_8Tr_8Tt_{38}$ (Tr(Triel) = Al, Ga, In) and $B_8Tr_{16}Tt_{30}$ (B = Ba, Sr, Eu), which have "fully occupied" framework stoichiometries (27–32). In the same vein, the inclusion of pnictides (Pn = P, As) is also permitted in the framework when halogen atoms (Br, I) are incorporated as guest atoms (33, 34).

We have recently examined the Structure I clathrate (Na_8Si_{46}) in the Na–Si system using Rietveld analysis of powder X-ray diffraction data combined with quantitative ^{29}Si MAS NMR spectroscopy, and have demonstrated that the framework contained no vacancies (38, 39). This finding is consistent with the report that Na_8Si_{46} is electrically conducting with metallic behavior (21), where the "additional" electrons serve to populate the conduction band and provide the carriers for the electronic conductivity. This is consistent with band structure calculations (38, 40), which shows that a rigid-band-model picture holds. In a rigid-band model picture, the band structure of Na_8Si_{46} is nearly identical to that of pristine Si_{46}. The additional electrons from sodium merely occupy the formerly empty conduction states of Si_{46}, and the Fermi energy now moves into the conduction band.

It is then of immediate interest to determine the framework stoichiometry in the analogous compound, $K_{8-x}Si_{46-y}$, for which conflicting reports have appeared in the literature. In their original report, Cros *et al.* (21) found that "K_7Si_{46}" was metallic, indicating that the clathrate framework was fully stoichiometric, and that the alkali atoms were providing electrons to the conduction band rather than being localized at framework defects. However, a more recent determination in the discussion by Miller (35 (based on unpublished thesis work of J. Llanos, University of Stuttgart, 1989)) concludes that the compound is best formulated as "$K_8Si_{44}\square_2$" and is semiconducting, which would be more consistent with the Zintl-Klemm concept and in line with the observation of Zhao and Corbett (37). In this paper, we investigate the stoichiometry and the electrical conductivity of $K_{8-x}Si_{46-y}$ and extend our investigation to the Rb–Si member of the series to complete the investigation of known members of the alkali metal Structure I clathrate compounds known to form with silicon. To offer better insight into our study by way of contrast, we have also synthesized, characterized, and measured the temperature dependence of the conductivity of $K_{8-x}Ge_{46-y}$, believed to contain vacancies in the framework, which has been formulated as semiconducting "$(K^+)_8\ (Ge_{44}\square)^{8-}$" (35).

SAMPLE SYNTHESIS

The silicon clathrate samples for this study were synthesized from the corresponding silicides KSi or RbSi, which in turn were prepared by treating stoichiometric mixtures of the elements (K or Rb and Si) at 666°C (in a tantalum capsule and sealed in a steel bomb) for 24 h. The germanium clathrate was prepared from the germanide KGe, which in turn was prepared by treating stoichiometric mixtures of the elements K and Ge at 666°C (in a tantalum capsule and sealed in a steel bomb) for 24 h. Excess alkali was removed from the silicides or germanide by evaporation at 250°C under a vacuum of $\sim 10^{-5}$ Torr. The silicon clathrate samples were then prepared by evaporating the alkali atoms between 425 and 475°C at a pressure of $\sim 10^{-6}$ Torr and similarly between 350 and 380°C for the germanium clathrate. Powder X-ray diffraction patterns were collected on a Siemens D-5000 diffractometer (Cu$K\alpha$) from 2θ = 5–90° (0.01° steps) with a scan rate of 1°/min. Structure refinements were carried out using the General Structure Analysis System (GSAS) for Rietveld profile analysis (41). Background coefficients, scale factor, peak shapes (pseudo-Voigt), atomic coordinates, unit cell constants, thermal parameters, and site occupancies were all refined. For conductivity data, samples were cold pressed into thin discs to between 85 and 90% of the theoretical density. Contacts were made by spring-loaded leads and silver paint was used as a "glue". Four-probe conductivity data based on the van der Pauw method (42, 43) in the range 80–600 K were collected for each of the clathrates studied in this report, by alternatively passing a current across two leads and measuring the voltage across the other two. The quality of the samples degraded (as indicated by broadening of the X-ray peaks, and the appearance of elemental Si or Ge peaks) when high-temperature conductivity measurements were performed in air. Subsequently, all measurements were performed under a flowing stream of nitrogen.

RESULTS AND DISCUSSION

A detailed quantitative measure of the framework site occupancy was obtained by carrying out full profile Rietveld analysis of the X-ray powder data sets. In Figs. 2 and 3 are shown the X-ray diffraction patterns, along with the theoretical and difference profiles, of the two silicon clathrates $K_{8-x}Si_{46-y}$ and $Rb_{8-x}Si_{46-y}$. In Tables 1 and 2 the lattice parameters, partial site coordinates, site occupancies,

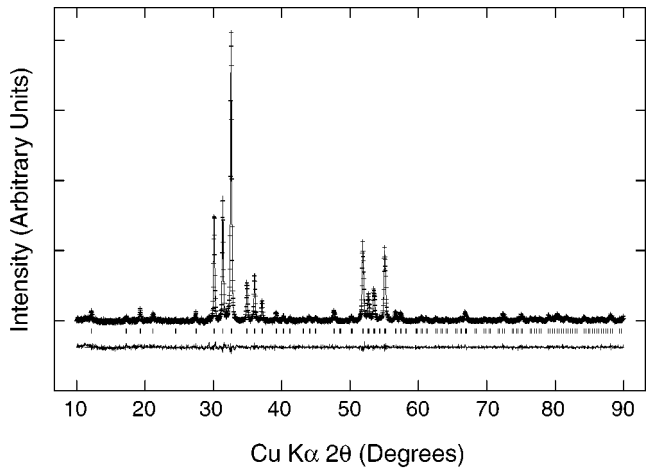

FIG. 2. Full profile Rietveld analysis of the powder X-ray diffraction pattern of K_8Si_{46}. Experimental data points are shown as pluses (+) and theoretical fits are shown as solid curves. Tick marks below the fit corresponds to the position of the Bragg reflections expected for the structure. Also shown below the fit is the difference between the observed and theoretical patterns.

and thermal parameters are collected for $K_{8-x}Si_{46-y}$ and $Rb_{8-x}Si_{46-y}$, respectively. The refined values of bond lengths and angles for $K_{8-x}Si_{46-y}$ and $Rb_{8-x}Si_{46-y}$ are collected in Tables 3 and 4. Figure 4 depicts the X-ray diffraction pattern of the germanium clathrate along with the theoretical and difference profiles. Data on lattice parameters, partial site coordinates, site occupancies, and thermal parameters are collected in Table 5. Table 6 summarizes the relevant information on the bond lengths, and Table 7

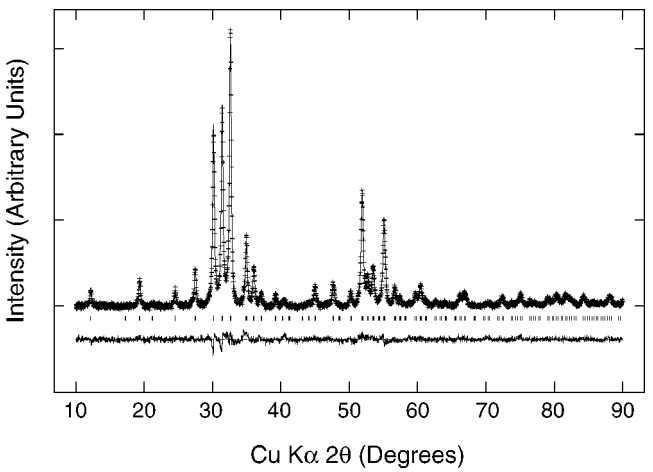

FIG. 3. Full profile Rietveld analysis of the powder X-ray diffraction pattern of Rb_6Si_{46}. Experimental data points are shown as pluses (+) and theoretical fits are shown as solid curves. Tick marks below the fit corresponds to the position of the Bragg reflections expected for the structure. Also shown below the fit is the difference between the observed and theoretical patterns.

TABLE 1
Atomic Positions, Site Occupancies, and Atomic Displacement Parameters for K_8Si_{46}

Atom	Site	x	y	z	Occupancy	100 U_{iso} (Å^2)
Si1	6*c*	$\frac{1}{4}$	0	$\frac{1}{2}$	1.006(9)	3.64(6)
Si2	16*i*	0.1848(2)	0.1848(2)	0.1848(2)	1.010(5)	3.64(6)
Si3	24*k*	0	0.3063(2)	0.1186(5)	1.018(2)	3.64(6)
K1	2*a*	0	0	0	0.885(4)	3.2(2)
K2	6*d*	$\frac{1}{4}$	$\frac{1}{2}$	0	0.975(3)	3.6(2)[a]

Note. Figure 2, 10,167 data points, $a = 10.27518(5)$, $\chi^2 = 1.491$, $R_p = 0.041$, $R_{wp} = 0.052$.

[a] $U_{11} = 4.067(341)$ Å^2, $U_{22} = 3.363(197)$ Å^2, $U_{33} = 3.363(197)$ Å^2, $U_{ij} = 0$ Å^2 ($i \neq j$).

the bond angles for the germanium clathrate. The variation of conductivity with temperature for $K_{8-x}Si_{46-y}$ and $Rb_{8-x}Si_{46-y}$ are collectively presented in Fig. 5. For the germanium clathrate, the variation of conductivity with temperature is presented in Fig. 6.

We discuss first the trends in framework–atom occupancies, the presence or absence of vacancies, and later in this section trends in the bond lengths and bond angles. In the context of these observations we then build the relationship with the observed conductivities. Clearly, based on the site occupancies of the framework atoms (Tables 1 and 2), both the K- and the Rb-based silicon clathrates are stoichiometric in the framework. For $K_{8-x}Si_{46-y}$ residuals obtained were $R_p = 4.1\%$ and $R_{wp} = 5.2\%$ and a χ^2 (goodness-of-fit) value of 1.49. Similar residuals for $R_{8-x}Si_{46-y}$ were $R_p = 2.9\%$ and $R_{wp} = 3.7\%$ and a χ^2 value of 1.77. Imposing vacancies at one-third of the 6*c* sites resulted in much larger values of residuals for both members, $K_{8-x}Si_{46-y}$ and $Rb_{8-x}Si_{46-y}$. For $K_{8-x}Si_{46-y}$ these residuals were $R_p = 6.17\%$ and $R_{wp} = 8.38\%$, with $\chi^2 = 3.19$, while for $Rb_{8-x}Si_{46-y}$ the residuals were $R_p = 4.72$ and $R_{wp} = 6.19\%$, with $\chi^2 = 3.76$. From this we readily

TABLE 2
Atomic Positions, Site Occupancies, and Atomic Displacement Parameters for Rb_6Si_{46}

Atom	Site	x	y	z	Occupancy	100 U_{iso} (Å^2)
Si1	6*c*	$\frac{1}{4}$	0	$\frac{1}{2}$	0.995(1)	1.42(3)
Si2	16*i*	0.1843(2)	0.1843(2)	0.1843(2)	1.013(5)	1.42(3)
Si3	24*k*	0	0.3037(4)	0.1186(8)	1.004(2)	1.42(3)
Rb1	2*a*	0	0	0	0.218(5)	4.1(1)
Rb2	6*d*	$\frac{1}{4}$	$\frac{1}{2}$	0	0.952(7)	2.54(9)[a]

Note. Figure 3, 10,167 data points, $a = 10.27188(6)$, $\chi^2 = 1.769$, $R_p = 0.029$, $R_{wp} = 0.037$.

[a] $U_{11} = 3.331(219)$ Å^2, $U_{22} = 2.132(110)$ Å^2, $U_{33} = 2.132(110)$ Å^2, $U_{ij} = 0$ Å^2 ($i \neq j$).

TABLE 3
Bond Distances in the Two Si_{46} Structures

	K_8Si_{46} (Å)	Rb_6Si_{46} (Å)
Si1–4Si3[a]	2.41015(1)	2.42628(1)
Si2–1Si2	2.32559(1)	2.33677(1)
Si2–3Si3	2.37105(2)	2.35396(1)
Si3–1Si1	2.41015(1)	2.42628(1)
Si3–2Si2	2.37105(2)	2.35396(1)
Si3–1Si3	2.42807(1)	2.43632(1)
Si1–A2[b]	3.63282(2)	3.63107(1)
Si2–A1	3.28649(1)	3.27875(1)
Si2–A2	3.81438(2)	3.81442(3)
Si3–A1	3.37048(1)	3.34815(1)
Si3–A2	3.47074(1)	3.48457(2)
Si3–A2	3.96553(1)	3.95553(1)

[a] The number before the atoms represents the multiplicity.
[b] A1, Alkali metal (K or Rb) at the 2*a* sites (center of Si_{20}); A2, alkali metal at the 6*d* sites (center of Si_{24}). For comparison, the bond length in elemental silicon is 2.35 Å.

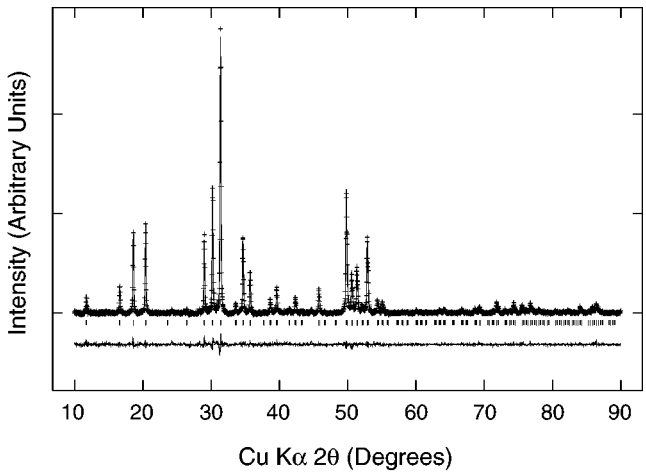

FIG. 4. Full profile Rietveld analysis of the powder X-ray diffraction pattern of $K_8Ge_{44}\square_2$. Experimental data points are shown as pluses (+) and theoretical fits are shown as solid curves. Tick marks below the fit corresponds to the position of the Bragg reflections expected for the structure. Also shown below the fit is the difference between the observed and theoretical patterns.

conclude that (a) both the silicon clathrates are *devoid* of framework vacancies and (b) the stoichiometries of the two silicon clathrates are K_8Si_{46} and Rb_6Si_{46}.

The germanium clathrate framework, however, *bears* vacancies (Table 5), and as observed in the tin clathrates, one-third of the 6*c* sites are vacant. The residuals for the germanium clathrate were $R_p = 3.5\%$ and $R_{wp} = 4.5\%$ with a χ^2 value of 1.95. Upon imposing full occupancy of the 6*c* sites (the *reverse* of what was done for the silicon clathrates), the residuals rose to $R_p = 5.3\%$ and $R_{wp} = 8.2\%$ with a χ^2 value of 6.07, establishing the presence of vacancies in this structure. At this stage we conclude from the refined X-ray data that the stoichiometry of the vacancy bearing germanium clathrate is K_8Ge_{44} (i.e., $K_8Ge_{44}\square_2$).

We now turn attention to the trends in bond angles and lengths. In the case of K_8Si_{46}, the K atoms both in the larger and smaller cages are nearly[2] completely filled (Table 1). In the case of Rb_6Si_{46}, the larger Si_{24} cages are nearly filled completely; however, the occupancy of the smaller Si_{20} cages substantially differs from unity (Table 2). An explanation for this may be offered (21) by choosing the van der Waal's radius of Si ($\sim$2.10 Å) to evaluate the "effective" radius available for the Rb atoms. From the refined data, the Rb–Si distances in the smaller Si_{20} cage are 3.27875(1) and 3.34815(1) Å (Table 3). We obtain, upon subtraction, "effective" radii of approximately 1.18 and 1.25 Å. Even the ionic radius of Rb (1.49 Å) is too large to easily enable accommodation of Rb atoms in the smaller cages. This explains the low observed occupancy for the Rb atoms in the 2*a* sites (see Table 2). Although the combined use of van der Waal's and ionic radii gives useful insights into the filling scheme, we wish to impress a word of caution. In ^{23}Na NMR experiments on Na_xSi_{136} and Na_8Si_{46} clathrates, large paramagnetic (Knight) shifts are observed for the sodium nuclei inside the cages (44–49). This observation precludes a simple description of the guest species as simple ions; they are likely better described as intermediate between "metallic" and "atomic" species, for effective size considerations.

The average Si–Si bond length in K_8Si_{46} is 2.390 Å and in Rb_6Si_{46} it is 2.392 Å (compared with 2.35 Å in diamond-structured Si). There is also a narrow distribution of bond lengths ($\delta d \sim 0.10$ Å, or 4.2%) in both structures. In the case

TABLE 4
Bond Angles[a] in the Two Si_{46} Structures

	K_7Si_{46}	Rb_6Si_{46}
Si3–Si1–Si3	108.419°(1)	108.018°(1)
Si3–Si1–Si3	111.597°(1)	112.419°(1)
Si2–Si2–Si3	108.956°(1)	109.219°(1)
Si3–Si2–Si3	109.981°(1)	109.722°(1)
Si1–Si3–Si2	105.836°(1)	105.861°(1)
Si1–Si3–Si3	124.202°(1)	123.791°(1)
Si2–Si3–Si2	106.310°(1)	107.061°(1)
Si2–Si3–Si3	106.752°(1)	106.659°(1)

[a] For comparison, the bond angle in elemental silicon is the tetrahedral angle of 109.47°.

[2] The phrases "nearly full" and "nearly empty" are used for the occupancies of the guest metal atoms, with respect to the occupancy of the framework sites.

TABLE 5
Atomic Positions, Site Occupancies, and Atomic Displacement Parameters for $K_8Ge_{44}\square_2$

Atom	Site	x	y	z	Occupancy	100 U_{iso} (Å^2)
Ge1	6*c*	$\frac{1}{4}$	0	$\frac{1}{2}$	0.691(3)	3.99(22)
Ge2	16*i*	0.1833(3)	0.1833(3)	0.1833(3)	0.997(2)	3.99(22)
Ge3	24*k*	0	0.3151(2)	0.1148(4)	0.998(5)	3.99(22)
K1	2*a*	0	0	0	0.854(6)	3.5(2)
K2	6*d*	$\frac{1}{4}$	$\frac{1}{2}$	0	0.969(4)	4.5(1)[a]

Note. Figure 4, 9565 data points, $a = 10.66771(1)$, $\chi^2 = 1.949$, $R_p = 0.035$, $R_{wp} = 0.045$.

[a] $U_{11} = 3.836(303)$ Å^2, $U_{22} = 4.998(267)$ Å^2, $U_{33} = 4.998(267)$ Å^2, $U_{ij} = 0$ Å^2 ($i \neq j$).

TABLE 7
Bond Angles[a] in $K_8Ge_{44}\square_2$

Ge3–Ge1–Ge3	109.343°(1)
Ge3–Ge1–Ge3	109.727°(1)
Ge2–Ge2–Ge3	106.591°(1)
Ge3–Ge2–Ge3	112.191°(1)
Ge1–Ge3–Ge2	107.537°(1)
Ge1–Ge3–Ge3	125.136°(1)
Ge2–Ge3–Ge2	102.958°(1)
Ge2–Ge3–Ge3	105.802°(1)

[a] For comparison, the bond angle in elemental germanium is the tetrahedral angle of 109.47°.

of $K_8Ge_{44}\square_2$, the average bond length is 2.463 Å (compared with 2.45 Å in diamond-structured Ge), and the variation is larger ($\delta d \sim 0.13$ Å; 5.3%). Following Zhao and Corbett (37), the presence of vacancies in $K_8Ge_{44}\square_2$ allows its formulation as $(K^+)_8(3b\text{-}Ge^{-1})_8(4b\text{-}Ge^0)_{36}$, where 3b stands for 3-bonded and 4b for 4-bonded Ge atoms. This formulation leads to the suggestion that different framework atoms are usefully described as existing in different oxidation states within the crystal. The longer average bond length and greater bond length distribution in the vacancy-bearing Ge-clathrates compared with the stoichiometric Si-clathrates is because of the presence of longer bonds involving the 3-bonded Ge atoms. In Fig. 7, we schematically show how each framework atom in the structure is bonded to others. Since vacancies form at the 6*c* sites, the presence of the lone pairs is most felt by atoms at the 24*k* sites (Ge3), (formulated as $3b\text{-}Ge^{-1}$ above, Fig. 7a). Bonds formed to these atoms are expected to be the longest, i.e., bonds between the atoms at 24*k* and 16*i* (Ge3–Ge2, Fig. 7b) and bonds between atoms at 24*k* and 24*k* (Ge3–Ge3, Fig. 7c). Indeed, the longest bonds in $K_8Ge_{44}\square_2$ are Ge3–Ge3 and Ge3–Ge2 (Table 6), in contrast to the case for the two silicon clathrates (Table 3). The same bond length pattern as in $K_8Ge_{44}\square_2$ is observed for the vacancy bearing Sn clathrates (37).

TABLE 6
Bond Distances (Å) in $K_8Ge_{44}\square_2$

Ge1–4Ge3[a]	2.41820(1)
Ge2–1Ge2	2.46280(1)
Ge2–3Ge3	2.50004(1)
Ge3–1Ge1	2.41820(1)
Ge3–2Ge2	2.50004(1)
Ge3–1Ge3	2.55037(1)
Ge1–K2	3.77160(2)
Ge2–K1	3.38785(1)
Ge2–K2	3.96753(2)
Ge3–K1	3.59037(1)
Ge3–K2	3.55659(1)
Ge3–K2	4.11679(1)

[a] The number before the atoms represents the multiplicity. For comparison, the bond angle in elemental germanium is 2.45 Å.

In the vacancy-containing germanium and tin compounds, one-third of the atoms at the 6*c* sites are missing, and the structures can be classified as defect-stabilized frameworks obeying the Zintl-Klemm rules, or as Zintl salts. The temperature dependence of electrical conductivity and magnetic susceptibility are consistent with the classification of these compounds as semiconducting and diamagnetic Zintl compounds (35–37). In contrast with this behavior, K_8Si_{46} and Rb_6Si_{46} exhibit conductivities (10^1–10^2 mho cm^{-1}) with a weak temperature dependence that are more typical of poor metals (Fig. 5). These values are consistent with earlier measurements of Cros *et al.* (21). For comparison, we have also measured the conductivity of our $K_8Ge_{44}\square_2$ sample. The conductivity increases steeply with increasing temperature and the semiconducting behavior is apparent in Fig. 6. The room temperature conductivity had a magnitude of $\sim 10^0$ mho cm^{-1} and the limiting high-temperature activation energy[3] is estimated as $E_a \sim 0.15$ eV.

A chemical description of the vacancy formation in the clathrate structures involves breaking bonds around the 6*c* framework sites. The "extra" electrons donated by the alkali atoms then form "lone pairs" directed toward the defect (35, 36). In this case, the electron pairing and localization energy must outweigh the energy required to break covalent bonding between tetrelide atoms to form the defect sites. This process is obviously favorable for the Ge and Sn clathrates, where the *Tt*–*Tt* bonding is weaker. In the case

[3] Although the limiting high-temperature activation energy (E_a) was estimated by plotting $-\log(\sigma)$ against $1/2k_BT$, it should be kept in mind that this gap reflects the energy difference between the "defect" states and the conduction band minimum. Contrast this with the band gap (2 eV) of pristine Ge_{46} estimated from theoretical considerations (59).

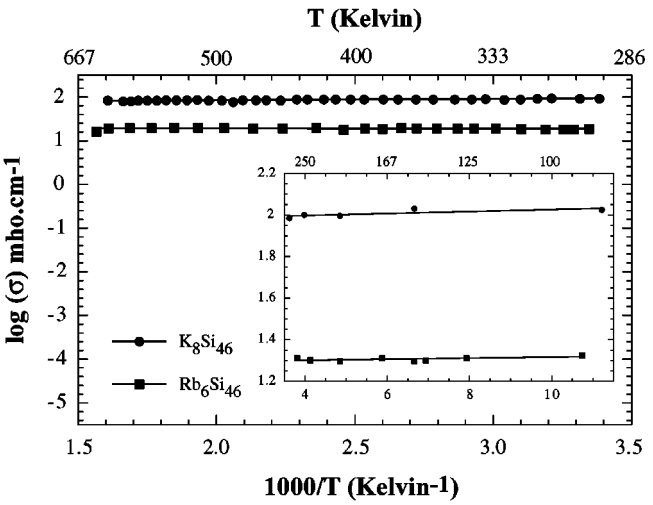

FIG. 5. Electrical conductivity of the two stoichiometric silicon clathrates K_8Si_{46} and Rb_6Si_{46}. The low-temperature data are presented in the inset and have the same units as the main figure. Over the temperature range (80–700 K) both samples exhibit metallic behavior.

of silicon clathrates, however, the Si–Si bonds are stronger, and the "extra" electrons from the guest atoms (Na, K, or Rb) are distributed in the conduction bands of the silicon framework. This results in the observed metallic conductivities and also gives rise to large Knight-like ^{29}Si NMR shifts for framework atoms, reminiscent of metals (38, 44, 48, 49). It is also possible to understand the vacancy formation in terms of a simplified band picture (Fig. 8). This leads to the formation of ("dangling" bonds) defect states in the gap where the "extra" electrons contributed by the guest become localized (35). This model allows

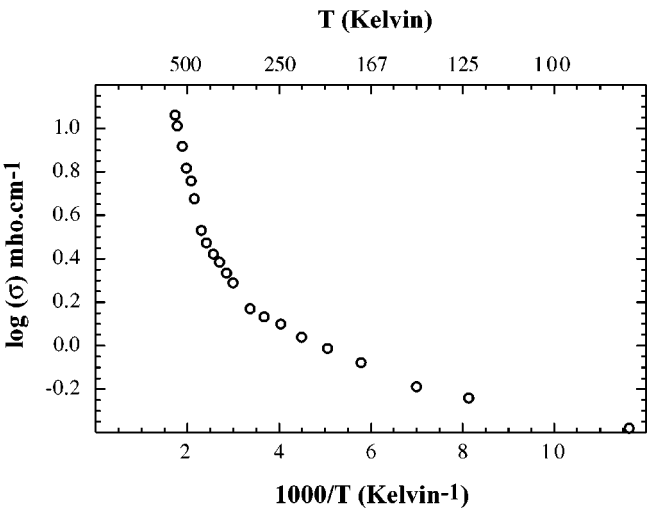

FIG. 6. Electrical conductivity of the vacancy bearing germanium clathrate $K_8Ge_{44}\square_2$. The material is semiconducting, with a thermal activation energy, E_a, estimated as $\sim$0.15 eV from the limiting high-temperature data.

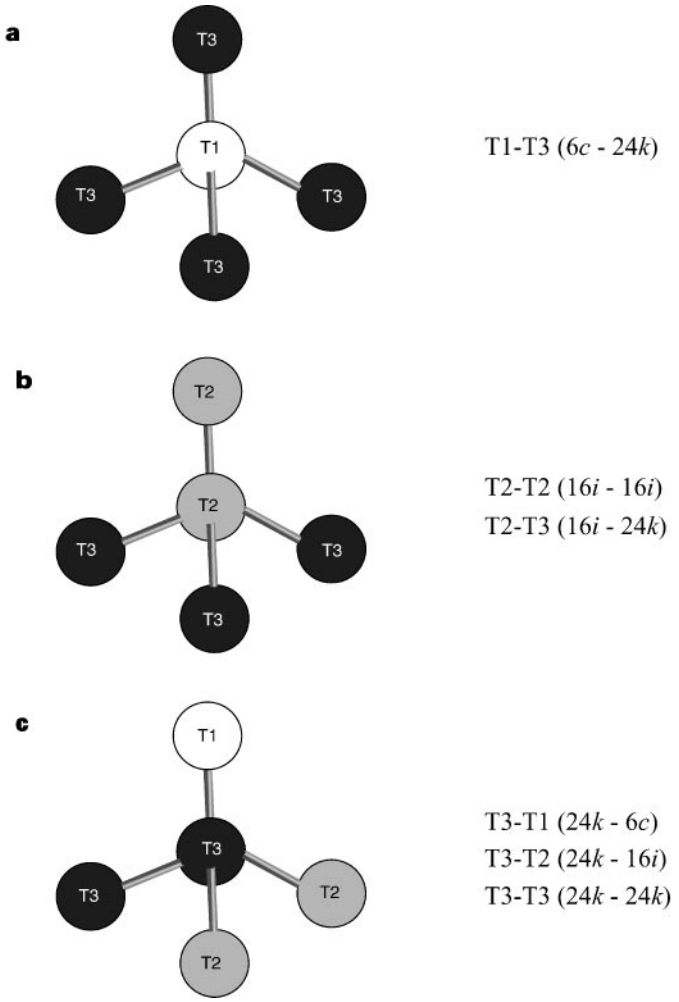

FIG. 7. Connectivity of the three crystallographically inequivalent tetrahedral atoms in the Structure I clathrate (see Fig. 1). The T1 (atoms at the 6*c* sites) have a site symmetry 4*m*2; the T2 (atoms at the 16*i* sites) have a site symmetry 3; and the atoms T3 (atoms at the 24*k* sites) have a site symmetry *m*. The tetrahedra are not ideal as in the diamond structure, but are distorted with angles ranging from 102° to 126° (see Table 4 and 7).

rationalization of the small band gap observed for the semiconducting "defect-stabilized" Ge and Sn clathrates. A detailed theoretical analysis of the energetics of vacancy formation and its effect upon the band structure will be presented elsewhere (50).

It has also been reported that clathrates in the $Na_2Ba_6Si_{46}$ and $K_xBa_ySi_{46}$ series, including Ba_8Si_{46}, do not contain vacancies (19, 51–53). These compounds are interesting because of the relatively high T_c (4–8 K) reported for sp^3-bonded structures (1, 19), thought to be associated with a concentration in *d*-electron density at the Fermi level derived from the Ba atoms (54, 55). Here the "extra" electron count is very large ($>$14 additional electrons provided by the alkali and alkaline earth atoms), and yet vacancies do not appear to be formed within the Si framework. Recent structural studies of Structure II silicon clathrates also

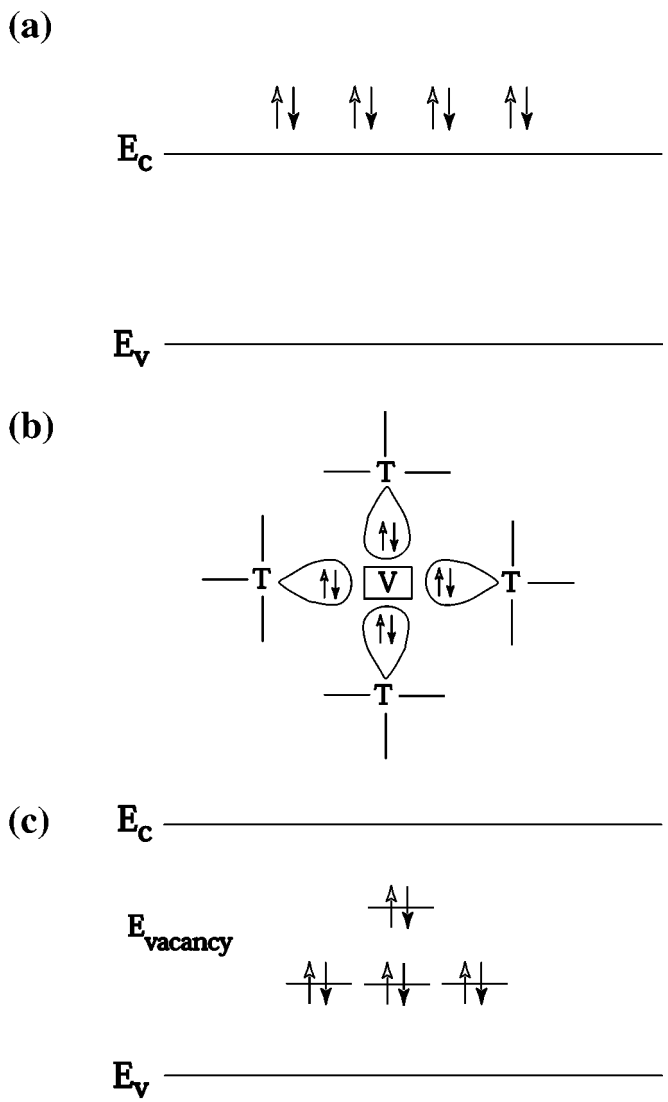

FIG. 8. Schematics for understanding the structure–conductivity relationship in binary Structure I clathrates. (a) In the case of K_8Si_{46}, the guest electrons populate the conduction states of pristine Si_{46}, resulting in metallic behavior (the valence and conduction states of Si_{46} are shown as E_v and E_c, respectively). (b) The chemical formulation for vacancy bearing clathrates, as suggested by (35–37), is shown. This formulation leads to the understanding of these materials as ionic-Zintl phases, with 3-bonded and 4-bonded sites within the structure. Lone electron pairs are supported by the atoms around the vacancies (marked as "V"). (c) A schematic band-picture model for $K_8Ge_{44}\square_2$: bond breaking around the atoms at the 6*c* sites results in defect states being formed within the bandgap of pristine Ge_{46}. These defect states are lower in energy than the conduction states (E_c and above) and are occupied by electrons from the guest atoms. In the case of the germanium clathrate, the combined process — bond breaking and lowering of guest electrons' energy is a favorable process due to weaker Ge–Ge bonds, in contrast to the silicon members where the Si–Si bond is much stronger.

indicate that none of the Na_xSi_{136} ($0 < x < 24$) members bear vacancies at the framework sites (39, 56). Here the higher ($x > 10$) members of the series are described as metallic (21). A single crystal structure refinement of the recently synthesized $Na_{16}Cs_8Si_{136}$ has showed this compound to be vacancy-free and metallic (57). These observations are all consistent with the arguments presented above, that Si clathrates do not appear to follow Zintl-Klemm rules for compound formation, presumably because of the strength of the Si–Si bond.

There are some intriguing recent results that suggest that similar behavior may also be observed in Ge-clathrates, however. A single-crystal study of $Na_{16}Cs_8Ge_{136}$ found this phase to be both stoichiometric and metallic (57). Among the substituted variants, $Ba_8Ga_{16}Ge_{30}$ (58) was reported to be superconducting (4–7 K) with metallic conductivity at ambient conditions. Within the Zintl-Klemm framework, we would expect that transfer of electrons from Ba to Ga should render the compound semiconducting like the closely related $Sr_8Ga_{16}Ge_{30}$, $Eu_8Ga_{16}Ge_{30}$, etc. (8, 9, 27, 28). Iversen *et al.* (13) recently found that there is in fact little charge transfer between Sr atoms and the Ga-Ge framework in $Sr_8Ga_{16}Ge_{30}$ clathrate.

In conclusion, the Zintl-Klemm concept provides a simple and elegant way of accounting both for the electron count and property of several clathrate compounds. However, as discussed above, exceptions are apparent, and the richness of complexity in bonding presented by the tetrelide clathrates is striking. This perhaps offers new opportunities to tailor novel material properties in these unique phases.

CONCLUSIONS

We report the synthesis and structural characterization of two Structure I silicon clathrates, K_8Si_{46} and Rb_6Si_{46}. Rietveld analysis of the powder diffraction data indicates that both compounds have fully occupied framework sites, and no tetrahedral vacancies are present within experimental error. This is consistent with previous results for Na_8Si_{46}. The "extra" electrons from the guest alkali atoms result in metallic conductivities for both K_8Si_{46} and Rb_6Si_{46}. Comparing these findings with the stoichiometries of the analogous K- and Rb (Ge and Sn)-clathrates suggests that the tendency to form vacancies should directly be borne out of the relative energetics involved in breaking bonds versus the stability gained by reducing the energy of the "extra" electrons in the conduction bands. The stoichiometry of the germanium clathrate is determined as $K_8Ge_{44}\square_2$ and, in accord with previous studies, is observed to be semiconducting with a narrow band gap of 0.15 eV.

ACKNOWLEDGMENTS

We acknowledge the NSF MRSEC award, DMR 96-32635, for financial support and Professor Jan Gryko for valuable discussions.

REFERENCES

1. H. Kawaji, H. Horie, H. Nakano, and M. Ishikawa, *Phys. Rev. Lett*. **74,** 1427 (1995).
2. G. B. Adams, M. O'Keeffe, A. A. Demkov, O. F. Sankey, and Y. Huang, *Phys. Rev. B* **49,** 8048 (1994).
3. A. A. Demkov, W. Windl, and O. F. Sankey, *Phys. Rev. B* **53,** 11,288 (1996).
4. A. A. Demkov, O. F. Sankey, K. E. Schmidt, G. B. Adams, and M. O'Keeffe, *Phys. Rev. B* **50,** 17,001 (1994); V. I. Smelyansky and J. S. Tse, *Chem. Phys. Letts.* **264,** 459 (1997).
5. E. Galvani, G. Onida, S. Serra, and G. Benedek, *Phys. Rev. Lett*. **77,** 3573 (1996).
6. J. Gryko, P. F. McMillan, R. F. Marzke, G. K. Ramachandran, D. Patton, S. K. Deb, and O. F. Sankey, in press.
7. G. A. Slack, *Mater. Res. Soc. Symp. Proc.* **478,** 47 (1997); G. A. Slack, *Solid State Phys.* **34,** 1 (1978).
8. G. Nolas, J. L. Cohn, G. A. Slack, and S. B. Schujman, *Appl. Phys. Lett*. **73,** 178 (1998).
9. J. L. Cohn, G. S. Nolas, V. Fessatidis, T. H. Metcalf, and G. A. Slack, *Phys. Rev. Lett*. **82,** 779 (1999).
10. G. S. Nolas, T. J. R. Weakley, and J. L. Cohn, *Chem. Mater*. **11,** 2470 (1999).
11. S. B. Shujman, G. S. Nolas, R. A. Young, C. Lind, A. P. Wilkinson, G. A. Slack, R. Patschke, M. G. Kanatzidis, M. Ulutagay, and S.-J. Hwu, *J. Appl. Phys.* **87,** 1529 (2000).
12. N. P. Blake, L. Mollnitz, G. Kresse, and H. Metiu, *J. Chem. Phys.* **111,** 3133 (1999).
13. B. B. Iversen, A. E. C. Palmqvist, D. E. Cox, G. S. Nolas, G. D. Stucky, N. P. Blake, and H. Metiu, *J. Solid State Chem.* **149,** 455 (2000).
14. B. C. Chakoumakos, B. C. Sales, D. G. Mandrus, and G. S. Nolas, *J. Alloys Comp.* **296,** 80 (2000).
15. J. Dong, O. F. Sankey, G. K. Ramachandran, and P. F. McMillan, *J. Appl. Phys.* **87,** 7726 (2000); J. S. Tse, K. Uehara, R. Rousseau, A. Ker, C. I. Ratcliffe, M. A. White, and G. Mackay, *Phys. Rev. Lett*. **85,** 114 (2000).
16. J. Dong, O. F. Sankey, A. A. Demkov, G. K. Ramachandran, J. Gryko, P. F. McMillan, and W. Windl, *Mater. Res. Soc. Symp. Proc.* **545,** 443 (1999).
17. G. K. Ramachandran, P. F. McMillan, S. K. Deb, M. Somayazulu, J. Dong, and O. F. Sankey, *J. Phys. Condens. Matter* **12,** 4013 (2000).
18. A. San-Miguel, P. Kéghélian, X. Blasé, P. Mélinon, A. Perez, J. P. Itié, A. Polian, E. Reny, C. Cros, and M. Pouchard, *Phys. Rev. Lett*. **83,** 5290 (1999).
19. S. Yamanaka, E. Enishi, H. Fukuoka, and M. Yasukawa, *Inorg. Chem.* **39,** 56 (2000).
20. J. S. Kasper, P. Hagenmuller, M. Pouchard, and C. Cros, *Science* **150,** 1713 (1965).
21. C. Cros, M. Pouchard, and P. Hagenmuller, *J. Solid State Chem.* **2,** 570 (1970).
22. C. Cros, M. Pouchard, P. Hagenmuller, and J. S. Kasper, *Bull. Soc. Chim. Fr*. **7,** 2737 (1968).
23. C. Cros, M. Pouchard, and P. Hagenmuller, *Comput. Red. Acad. Sci.* **260,** 4764 (1965).
24. J. Gallmeier, H. Schäfer, and A. Weiss, *Z. Naturforsch.* **22b,** 1080 (1967).
25. J. Gallmeier, H. Schäfer, and A. Weiss, *Z. Naturforsch.* **24b,** 665 (1969).
26. M. O'Keeffe, G. B. Adams, and O. F. Sankey, *Philos. Mag. Lett*. **78,**21 (1998).
27. B. Eisenmann, H. Schafer, and R. Zagler, *J. Less-Common Met*. **118,** 43 (1986).
28. G. Cordier and P. Woll, *J. Less-Common Met*. **169,** 291 (1991).
29. R. Kröner, K. Peters, H. G. von Schnering, and R. Nesper, *Z. Kristallogr.* **213,** 667 (1998).
30. R. Kröner, K. Peters, H. G. von Schnering, and R. Nesper, *Z. Kristallogr.* **213,** 669 (1998).
31. H. G. von Schnering, H. Memke, R. Kröner, K. Peters, and R. Nesper, *Z. Kristallogr.* **213,** 673 (1998).
32. R. Kröner, K. Peters, H. G. von Schnering, and R. Nesper, *Z. Kristallogr.* **213,** 675 (1998).
33. T. L. Chu, S. S. Chu, and R. L. Ray, *J. Appl. Phys.* **53,** 7102 (1982).
34. M. M. Shatruk, K. A. Kovnir, A. V. Shevelkov, I. A. Presniakov, and B. A. Popovkin, *Inorg. Chem.* **38,** 3455 (1999).
35. See the chapters by G. Miller and J. D. Corbett *in* "Chemistry, Structure and Bonding of Zintl Phases and Ions," (S. M. Kauzlarich (Ed.)), VCH, New York, 1996.
36. H. G. von Schnering, *Nova Acta Leopold*. **59,** 168 (1985).
37. J.-T. Zhao and J. D. Corbett, *Inorg. Chem.* **33,** 5721 (1994).
38. G. K. Ramachandran, P. F. McMillan, J. Diefenbacher, J. Gryko, J. Dong, and O. F. Sankey, *Phys. Rev. B* **60,** 12,294 (1999).
39. G. K. Ramachandran, J. Dong, J. Diefenbacher, J. Gryko, R. F. Marzke, O. F. Sankey, and P. F. McMillan, *J. Solid State Chem.* **145,** 716 (1999).
40. K. Moriguchi, M. Yonemura, A. Shintani, and S. Yamanaka, *Phys. Rev. B* **61,** 9859 (2000).
41. Larson and R. B. von Dreele, GSAS—Generalized Structure Analysis System, LANSCE, MS-H805, Manual Lujan Neutron Scattering Center, Los Alamos, NM, 1989.
42. L. J. van der Pauw, *Philips Res. Rep.* **13,** 1 (1958).
43. L. J. van der Pauw, *Philips Tech. Rev*. **20,** 220 (1958–1959).
44. J. Gryko, P. F. McMillan, and O. F. Sankey, *Phys. Rev. B* **54,** 3037 (1996).
45. J. Gryko, P. F. McMillan, R. F. Marzke, A. P. Dodokin, A. A. Demkov, and O. F. Sankey, *Phys. Rev. B* **57,** 4172 (1998).
46. E. Reny, M. Menetrier, C. Cros, M. Pouchard, and J. Senegas, *C. R. Acad. Sci. Paris* **1,** 129 (1998).
47. G. K. Ramachandran, J. Diefenbacher, O. F. Sankey, R. Sharma, R. F. Marzke, M. O'Keeffe, J. Gryko, and P. F. McMillan, *Mater. Res. Soc. Symp. Proc.* **507,** 483 (1998).
48. Shimizu, Y. Maniwa, K. Kume, H. Kawaji, S. Yamanaka, and M. Ishikawa, *Phys. Rev. B* **54,** 13,242 (1996).
49. F. Shimizu, Y. Maniwa, K. Kume, H. Kawaji, S. Yamanaka, and M. Ishikawa, *Synth. Met*. **86,** 2141 (1997).
50. J. Dong *et al.* (in preparation); J. Dong and O. F. Sankey, *Phys. Rev. B* **60,** 950 (1999).
51. S. Yamanaka, H.-O. Horie, H. Kawaji, and M. Ishikawa, *Eur. J. Solid State Inorg. Chem.* **32,** 799 (1995).
52. S. Yamanaka, H.-O. Horie, H. Nakano, and M. Ishikawa, *Full. Sci. Tech.* **3,** 21 (1995).
53. H. Kawaji, K. Iwai, S. Yamanaka, and M. Ishikawa, *Solid State Commun.* **100,** 393 (1996).
54. S. Saito and A. Oshiyama, *Phys. Rev. B* **51,** 2628 (1995).
55. T. F. Fassler and C. Kronseder, *Angew. Chem. Int. Ed. Engl.* **36,** 2683 (1997).
56. E. Reny, P. Gravereau, C. Cros, and M. Pouchard, *J. Mater. Chem.* **8,** 2839 (1998).
57. S. Bobev and S. C. Sevov, *J. Am. Chem. Soc.* **121,** 3795 (1999).
58. The nominal compound $Ba_8Ga_{16}Ge_{30}$ has now been reported by different authors to have different transport properties, suggesting that a range of compositions is possible. All reports indicate that the material is semiconducting, barring the report by J. D. Bryan, V. I. Srdanov, G. D. Stucky, and D. Schmidt, *Phys. Rev. B* **60,** 3064 (1999). At ambient conditions, these authors observe metallic conductivity for $Ba_8Ga_{16}Ge_{30}$. Further, they report its superconductivity with a critical temperature of $\sim$4 K.
59. J. Dong and O. F. Sankey, *J. Phys. Condens. Matter* **11,** 6129 (1999).